Inorg. Chem. **2009**, *48*, 527−540

Generation of Ferryl Species through Dioxygen Activation in Iron/EDTA Systems: A Computational Study

Leonardo Bernasconi* and Evert Jan Baerends*

Theoretische Chemie, Vrije Universiteit Amsterdam, De Boelelaan 1083, 1081 HV Amsterdam, The Netherlands

Received May 31, 2008

The ferryl species (oxidoiron(IV), FeO^{2+}) is a ubiquitous, highly oxidative intermediate in oxidation catalysis. We study theoretically its abiotic generation, in the form of the singularly active complex of FeO^{2+} with the $EDTAH_n^{-4+n}$, $n = 0-4$ ligands, from O_2 and Fe^{2+}−EDTA complexes. The calculations are for the gas phase using generalized gradient corrected (BLYP and OPBE) Density Functional Theory (DFT). We examine the effects of ligand protonation on the coordination geometry and electronic structure of the chelated Fe^{2+} ion, on its affinity to bind dioxygen, and on the generation of dinuclear Fe/EDTA/O_2 complexes, whose formation has been hypothesized on the basis of kinetic measurements of Fe^{II}/Fe^{III} autoxidation reactions in aqueous solution. We also consider the homolytic cleavage of the O−O bond within one such complex, $[Fe \cdot EDTAH \cdot O_2 \cdot EDTAH \cdot Fe]^{2-}$, and we show that this reaction leads to a pair of $Fe^{IV}O$/EDTA systems with an energetic barrier comparable to those computed for model systems of active sites of enzymes involved in dioxygen activation, such as methane monooxygenase. Our study supports the recently advanced hypothesis that high valent iron compounds capable of oxidizing organic substrates may be produced as a byproduct of the Fe^{II}/Fe^{III} autoxidation in aqueous Fe/EDTA/O_2 solutions at ambient conditions. We also identify the origin of the enhanced O_2 activation ability in the monoprotonated $[Fe \cdot EDTAH]^-$ complex, compared to other ligand protonation states, which has been observed in kinetic measurements.

I. Introduction

The hydroxylation of saturated hydrocarbons at mild temperature and pressure conditions is an ambitious and tremendously far reaching goal. Several iron containing heme[1−8] and non-heme[9−13] enzymes are known (or have been postulated) to effect the conversion of hydrocarbons into OH-group containing species via high-valent Fe^{IV}-oxo (ferryl) intermediates. Ferryl complexes are strong oxidants, capable of direct H abstraction and hydroxylation of organic substrates.[14,15] Numerous experimental and computational studies on natural and synthetic (biomimetic or not) Fe^{IV}-oxo systems have shed light on the chemical mechanism explaining the ability of an Fe^{IV}-oxo moiety to activate even the strongest C−H bonds in most situations.[16−27] At the same

* To whom correspondence should be addressed. E-mail: l.bernasconi@few.vu.nl (L.B.), ej.baerends@few.vu.nl (E.J.B.).

(1) Groves, J. T. *J. Inorg. Biochem.* **2006**, *100*, 434–447.
(2) Bassan, A.; Blomberg, M. R. A.; Borowski, T.; Siegbahn, P. E. M. *J. Inorg. Biochem.* **2006**, *100*, 727–743.
(3) Debrunner, P. G. *Hyperfine Interact.* **1990**, *53*, 21–36.
(4) Rutter, R.; Valentine, M.; Hendrich, M. P.; Hager, L. P.; Debrunner, P. G. *Biochemistry* **1983**, *22*, 4769–4774.
(5) Rutter, R.; Hager, L. P.; Dhonau, H.; Hendrich, M.; Valentine, M.; Debrunner, P. *Biochemistry* **1984**, *23*, 6809–6816.
(6) Schulz, C. E.; Devaney, P. W.; Winkler, H.; Debrunner, P. G.; Doan, N.; Chiang, R.; Rutter, R.; Hager, L. P. *FEBS Lett.* **1979**, *103*, 102–105.
(7) Schulz, C. E.; Rutter, R.; Sage, J. T.; Debrunner, P. G.; Hager, L. P. *Biochemistry* **1984**, *23*, 4743–4754.
(8) Hersleth, H.-P.; Ryde, U.; Rydberg, P.; Görbitz, C. H.; Andersson, K. K. *J. Inorg. Biochem.* **2006**, *100*, 460–476.
(9) Price, J. C.; Barr, E. W.; Tirupati, B.; Bollinger, J. M., Jr.; Krebs, C. *Biochemistry* **2003**, *42*, 7497–7508.
(10) Price, J. C.; Barr, E. W.; Glass, T. E.; Krebs, C.; Bollinger, J. M., Jr. *J. Am. Chem. Soc.* **2003**, *125*, 13008–13009.
(11) Proshlyakov, D. A.; Henshaw, T. F.; Monterosso, G. R.; Ryle, M. J.; Hausinger, R. P. *J. Am. Chem. Soc.* **2004**, *126*, 1022–1023.
(12) Kryatov, S. V.; Rybak-Akimova, E. V.; Schindler, S. *Chem. Rev.* **2005**, *105*, 2175–2226.
(13) Solomon, E. I.; Brunold, T. C.; Davis, M. I.; Kemsley, J. N.; Lee, S.-K.; Lehnert, N.; Neese, F.; Skulan, A. J.; Yang, Y.-S.; Zhou, J. *Chem. Rev.* **2000**, *100*, 235–349.
(14) Kaizer, J.; Klinker, E. J.; Oh, N. Y.; Rohde, J.-U.; Song, W. J.; Stubna, A.; Kim, J.; Münck, E.; Nam, W.; Que, L., Jr. *J. Am. Chem. Soc.* **2003**, *126*, 472–473.
(15) Price, J. C.; Barr, E. W.; Glass, T. E.; Krebs, C.; Bollinger, J. M., Jr. *J. Am. Chem. Soc.* **2003**, *125*, 13008–13009.
(16) Shaik, S.; Filatov, M.; Schröder, D.; Schwarz, H. *Chem.−Eur. J.* **1998**, *4*, 193–199.
(17) Harris, N.; Shaik, S.; Schröder, D.; Schwarz, H. *Helv. Chim. Acta* **1999**, *82*, 1784–1797.

10.1021/ic800998n CCC: $40.75
Published on Web 12/15/2008

time, they have highlighted the complexity and variety of environmental effects affecting the catalytic efficiency of the Fe^{IV}-oxo group as a hydroxylation catalyst. These may range from electrostatic or chemical interaction with ligands coordinated to the metal center to subtle dielectric effects from the surrounding protein or solvent medium.

An Fe^{IV}-oxo complex has traditionally been regarded as a possible active species in the Fenton mixture (ferrous salts and hydrogen peroxide) whose oxidative properties are competitive in strength, if not in efficiency or specificity, with those of most hydroxylation enzymes.[1,28−33] Computational studies have confirmed the stability of a hydrated Fe^{IV}-oxo species, namely $[(H_2O)_5FeO]^{2+}$, in the gas phase, as well as in aqueous solution,[19,21,34−36] and a plausible mechanism through which $[(H_2O)_5FeO]^{2+}$ might be generated at room temperature from aqueous Fe^{2+}/H_2O_2 in typical Fenton conditions has been proposed on the basis of first-principles molecular dynamics simulations.[35,37,38] $[(H_2O)_5FeO]^{2+}$ has been synthesized (albeit in conditions dissimilar from those of classical Fenton chemistry)[36,39,40] and characterized chemically and spectroscopically.

Biological/biomimetic hydroxylations and (aqueous) Fenton chemistry offer two complementary perspectives on Fe^{IV}-oxo based reactivity and on the formation of ferryl species in different environments. The relative simplicity of processes leading to the generation of the catalytically active species in the Fenton reagent contrasts, however, with the complexity of the chemical processes involved in the formation of heme Fe^{IV}-oxo active centers in vivo. An example of the latter are the reactions mediated by the mitochondrial electron transport chain in aerobic respiration.[41] The essential difference between the two situations is that in biological chemistry the final acceptor of electrons for the oxidation of iron ions is dioxygen,

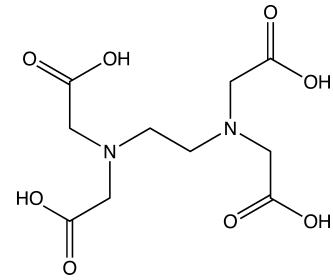

Figure 1. Structure of the four-time protonated (neutral) EDTA ligand.

$$Fe^{2+} + \frac{1}{2}O_2 \rightarrow Fe^{4+}O^{2-}$$

while in Fenton chemistry it is a hydrogen peroxide molecule,

$$Fe^{2+} + H_2O_2 \rightarrow Fe^{4+}O^{2-} + H_2O$$

The first process is thus associated to the *chemical activation* of a dioxygen molecule, involving the breaking of a fairly strong (493.4 kJ mol^{-1})[42] O−O bond, which occurs biologically in a sequence of steps. In this work we present an exploratory study of a realistic abiotic system in which a ferryl species might be plausibly generated by direct reaction of O_2 and Fe^{2+} in aqueous solution at ambient pressure and temperature conditions. Our work has been stimulated by recent experimental studies on the effect of chelators on the rate of autoxidation of Fe^{II} to Fe^{III} in solution.[43−46] These studies have put forward evidence for the generation of a strong oxidant, which is not the hydroxyl radical, if the reaction is carried out in the presence of EDTA ligand (Figure 1) and zerovalent iron. It has been suggested[43,45] that a hypervalent iron complex, for example, a ferryl or perferryl species can be generated in the course of the reaction, with a reduction potential of at least 1.2 V, that is, capable of oxidizing alcohols in aqueous solution.

The Fe^{II}-to-Fe^{III} autoxidation reaction in the presence of aqueous aminocarboxylate complexes and dioxygen has been extensively investigated by van Eldik and co-workers[47−50] (see also ref 46), and a multistep mechanism has been proposed on the basis of kinetic data. The reaction is initiated by the substitution of a coordinated water molecule by

(18) Schröder, D.; Shaik, S.; Schwarz, H. *Acc. Chem. Res.* **2000**, *33*, 139–145.
(19) Buda, F.; Ensing, B.; Gribnau, M. C. M.; Baerends, E. J. *Chem.—Eur. J.* **2001**, *7*, 2775–2783.
(20) Bassan, A.; Blomberg, M. R. A.; Siegbahn, P. E. M. *Chem.—Eur. J.* **2003**, *9*, 106–115.
(21) Buda, F.; Ensing, B.; Gribnau, M. C. M.; Baerends, E. J. *Chem.—Eur. J.* **2003**, *9*, 3436–3444.
(22) Decker, A.; Rohde, J.-U.; Que, L., Jr.; Solomon, E. I. *J. Am. Chem. Soc.* **2004**, *126*, 5378–5379.
(23) Ghosh, A.; Tangen, E.; Ryeng, H.; Taylor, P. R. *Eur. J. Inorg. Chem.* **2004**, *23*, 4555–4560.
(24) Schöneboom, J. C.; Neese, F.; Thiel, W. *J. Am. Chem. Soc.* **2005**, *127*, 5840–5853.
(25) Decker, A.; Clay, M. D.; Solomon, I. *J. Inorg. Biochem.* **2006**, *100*, 697–706.
(26) Neese, F. *J. Inorg. Biochem.* **2006**, *100*, 716–726.
(27) Yoshizawa, K. *Acc. Chem. Res.* **2006**, *39*, 375–382.
(28) Bray, W. C.; Gorin, M. H. *J. Am. Chem. Soc.* **1932**, *54*, 2124–2125.
(29) Groves, J. T.; Van Der Puy, M. *J. Am. Chem. Soc.* **1974**, *96*, 5274–5275.
(30) Groves, J. T.; McClusky, G. A. *J. Am. Chem. Soc.* **1976**, *98*, 859–861.
(31) Wardman, P.; Candeias, L. P. *Radiat. Res.* **1996**, *145*, 523–531.
(32) Dunford, H. B. *Coord. Chem. Rev.* **2002**, *233*, 311–318.
(33) Gozzo, F. *J. Mol. Catal. A: Chem.* **2001**, *171*, 1–22.
(34) Louwerse, M. J.; Baerends, E. J. *Phys. Chem. Chem. Phys.* **2007**, *9*, 156–166.
(35) Ensing, B.; Buda, F.; Blöchl, P.; Baerends, E. J. *Phys. Chem. Chem. Phys.* **2002**, *4*, 3619–3627.
(36) Pestovsky, O.; Stoian, S.; Bominaar, E. L.; Shan, X.; Münck, E.; Que, L., Jr.; Bakac, A. *Angew. Chem., Int. Ed.* **2005**, *44*, 6871–6874.
(37) Ensing, B.; Buda, F.; Blöchl, P.; Baerends, E. J. *Angew. Chem., Int. Ed.* **2001**, *40*, 2893–2895.
(38) Ensing, B.; Buda, F.; Gribnau, M. C. M.; Baerends, E. J. *J. Am. Chem. Soc.* **2004**, *126*, 4355–4365.
(39) Løgager, T.; Holcman, J.; Sehested, K.; Pedersen, T. *Inorg. Chem.* **1992**, *31*, 3523–3529.
(40) Pestovsky, O.; Bakac, A. *J. Am. Chem. Soc.* **2004**, *126*, 13757–13764.
(41) Babcock, G. T. *Proc. Nat. Acad. Sci. U.S.A.* **1999**, *96*, 12971–12973.
(42) Earnshaw, A.; Greenwood, N. In *Chemistry of the Elements*; Butterworth-Heinemann: Oxford, 1997.
(43) Englehardt, J. D.; Meeroff, D. E.; Echegoyen, L.; Deng, Y.; Raymo, F. M.; Shibata, T. *Environ. Sci. Technol.* **2007**, *41*, 270–276.
(44) Noradoun, C. E.; Cheng, I. F. *Environ. Sci. Technol.* **2005**, *39*, 7158–7163.
(45) Welch, K. D.; Davis, T. Z.; Aust, S. D. *Arch. Biochem. Biophys.* **2002**, *397*, 360–369.
(46) Gambardella, F.; Ganzeveld, I. J.; Winkelman, J. G. M.; Heeres, E. J. *Ind. Eng. Chem. Res.* **2005**, *44*, 8190–8198.
(47) Zang, V.; van Eldik, R. *Inorg. Chem.* **1990**, *29*, 1705–1711.
(48) Seibig, S.; van Eldik, R. *Inorg. Chem.* **1997**, *36*, 4115–4120.
(49) Seibig, S.; van Eldik, R. *Eur. J. Inorg. Chem.* **1999**, *1999*, 447–454.
(50) Seibig, S.; van Eldik, R. *Inorg. React. Mech.* **1999**, *1*, 91–105.

dioxygen in the more reactive once-protonated EDTA complex (notice unprotonated EDTA carries an overall −4 charge),

$$[Fe^{II}(EDTA)(H_2O)]^{2-} + H^+ \rightleftharpoons [Fe^{II}(EDTAH)(H_2O)]^- \quad (1)$$

$$[Fe^{II}(EDTAH)(H_2O)]^- + O_2 \rightleftharpoons [Fe^{II}(EDTAH)(O_2)]^- + H_2O \quad (2)$$

This is supposed to be followed by an intramolecular electron transfer, yielding a (formally) Fe^{III}-superoxide complex

$$[Fe^{II}(EDTAH)(O_2)]^- \rightarrow [Fe^{III}(EDTAH)(O_2^-)]^- \quad (3)$$

which by reaction with another $[Fe^{II}(EDTAH)(H_2O)]^-$ complex produces a dimeric peroxide complex

$$[Fe^{III}(EDTAH)(O_2^-)]^- + [Fe^{II}(EDTAH)(H_2O)]^- \rightarrow [(EDTAH^{3-})Fe^{III}(O_2^{2-})Fe^{III}(EDTAH)]^{2-} + H_2O \quad (4)$$

The latter is postulated to decompose rapidly to $[Fe^{III}(EDTAH)(H_2O)]$ and H_2O_2,

$$[(EDTAH)Fe^{III}(O_2^{2-})Fe^{III}(EDTAH)]^{2-} + 2H_2O + 2H^+ \rightarrow 2[Fe^{III}(EDTAH)(H_2O)] + H_2O_2 \quad (5)$$

The resulting H_2O_2 is held responsible for the oxidation of the excess $[Fe^{II}(EDTAH)(H_2O)]^-$,

$$2[Fe^{II}(EDTAH)(H_2O)]^- + H_2O_2 + 2H^+ \rightarrow 2[Fe^{III}(EDTAH)(H_2O)] + 2H_2O \quad (6)$$

However, no H_2O_2 was detected in the reaction mixture. This has been related to the large rate constant for the last reaction.[51,52]

In a recent study of iron-mediated oxidation of EDTA in aqueous solution,[43] Englehardt et al. have seized upon the possible presence of hydrogen peroxide in this reaction scheme and have advanced the hypothesis that an Fe^{IV}-oxo species could be formed as a byproduct of the above sequence of reactions. According to earlier computational results of Buda et al.,[19,35,37] the formation of an active Fe^{IV}-oxo intermediate from hydrogen peroxide may occur through the following steps:

$$H_2O_2 + [(H_2O)_6Fe^{II}]^{2+} \rightarrow [(H_2O)_5Fe^{II}(H_2O_2)]^{2+} + H_2O \quad (7)$$

$$[(H_2O)_5Fe^{II}(H_2O_2)]^{2+} \rightarrow [(H_2O)_4Fe^{IV}(OH)_2]^{2+} + H_2O \quad (8)$$

$$[(H_2O)_4Fe^{IV}(OH)_2)]^{2+} + H_2O \rightarrow [(H_2O)_5Fe^{IV}O]^{2+} + H_2O \quad (9)$$

The (pentaaqua complex of) FeO^{2+} would then be responsible for the oxidation of EDTA to glyoxylic acid and eventually formaldehyde, which has been observed at ambient temperature, pressure, and pH conditions. This same Fe^{IV}-oxo species can potentially also act as an oxidant for alcohols, consistent with the hypothesis of Welch et al.[45] This mechanism requires the presence of non-chelated ferrous ions, which in the experimental setup described by Englehardt et al. is made available by a continuous regeneration of Fe^{II} from oxidation of Fe^0.

It is, however, interesting to observe that the reactions of eqs 7−9 are not the only conceivable pathway to Fe^{IV}-oxo species. In a mechanism compatible with eqs 1−6, oxidation to Fe^{IV} might also occur through a direct cleavage of the dimeric peroxo complex of eqs 4 and 5:

$$[(EDTAH)Fe^{III}(O_2)Fe^{III}(EDTAH)]^{2-} \rightarrow 2[Fe^{IV}O(EDTAH)^-] \quad (10)$$

Reductive cleavage of the O−O bond is known to occur in enzymes containing dinuclear non-heme iron sites responsible for O_2 activation.[12,13] For instance, in the case of methane monooxygenase,[53] two different limiting mechanisms have been proposed for O−O bond breaking: (1) formation of a (side-on peroxo) biferric species, followed by homolytic O−O cleavage; (2) 2-fold protonation of one oxygen atom, followed by heterolytic O−O cleavage, with release of one water molecule (see ref 13 and refs therein). It is evident that none of these reactions involves the formation of H_2O_2, which offers an alternative explanation as to the reason why the latter species is not observed experimentally in the oxidation with O_2, whereas it should according to the postulated reactions 5 and 6.

The use of O_2 as primary oxygen source is of course highly desirable. If the occurrence of ferryl species and their involvement in oxidation processes is proved conclusively in the aqueous Fe/EDTA solutions, this might be the first artificial system capable of generating reactive high valent Fe compounds through dioxygen activation chemistry at mild temperature and pressure conditions. In this work we focus on the issue as to whether complexes similar to $Fe^{IV}O(EDTAH)^-$, that is, in which a *chelated* ferryl ion is generated from aerobic oxidation of a chelated Fe^{II} ion, may appear in typical experimental conditions. This is a particularly intriguing possibility because of prospective applications of systems of this kind to homogeneous hydroxylation catalysis. We have recently presented a study of the relation between reactivity, spin state, and electronic structure of Fe^{IV}-oxo complexes derived from $[(H_2O)_5Fe^{IV}O]^{2+}$ by progressive substitution of the water ligands.[54] Our work was based on Density Functional Theory (DFT) calculations performed on small gas-phase clusters, and was aimed at extending earlier findings about the importance of a low lying empty $3\sigma^*$ acceptor orbital in influencing the reactivity of $[(H_2O)_5Fe^{IV}O]^{2+}$ in alkane hydroxylations.[19,21,34] We were able to prove that oxygen rich, as opposed to, for example, nitrogen rich, equatorial (i.e., perpendicular to the Fe−O bond) coordination environments promote the reactivity of $Fe^{IV}O$ species by stabilizing a more reactive quintet ($S = 2$) ground state over the triplet ($S = 1$) one. Furthermore, the axial ligand *trans* to the oxo group should have little or no donor strength, to not destabilize the $3\sigma^*$ orbital. As a matter

(51) Bull, C.; McClune, G. J.; Fee, J. A. *J. Am. Chem. Soc.* **1983**, *105*, 5290–5300.
(52) Borggard, O. K.; Farver, O.; Andersen, V. S. *Acta Chem. Scand.* **1971**, *25*, 3541–3543.
(53) Lieberman, R. L.; Rosenzweig, A. C. *Nature* **2005**, *34*, 177–182.
(54) Bernasconi, L.; Louwerse, M. J.; Baerends, E. J. *Eur. J. Inorg. Chem.* **2007**, *2007*, 3023–3033.

of fact, the EDTA ligand is close to ideal, ligating the FeO^{2+} by equatorial oxygens from the four carboxylate groups, and having very weak axial donor strength because of the large distance of the two N lone pairs, which together act as *trans* axial ligand, from the Fe.[55] We will show here that Fe^{IV} complexes *in a high spin state* may indeed be generated through a process similar to the one described by eq 10, with O−O cleavage barriers comparable to those observed in biochemical processes of O_2 activation. On the basis of electronic structure considerations, we will also provide an explanation for the higher O_2 activation ability of the monoprotonated $[Fe{\cdot}EDTAH]^-$ complex, as compared to other ligand protonation states, which may be correlated to the observed higher autoxidation reaction rate at pH < 5.[48]

The paper is organized as follows. In Section II details regarding the calculations are provided. In Section IIIA we analyze the structure of Fe^{II}−EDTA in various ligand protonation states. In particular, we study how protonation of one or more carboxylate arms modifies the metal coordination environment and how this in turn affects the interaction with a coordinating dioxygen molecule and the ability to generate a dinuclear Fe/EDTA/O_2 complex. In Section IIIB we examine the electronic structure of the dinuclear complex $[Fe{\cdot}EDTAH{\cdot}O_2{\cdot}EDTAH{\cdot}Fe]^{2-}$ and in Section IIIC we show how the generation of two chelated ferryl species may take place via homolytic O−O bond breaking. Our results are summarized in Section IIID.

II. Computational Details

Calculations were performed using ADF[56−58] with a basis set of TZP quality for all atoms. All electrons were treated explicitly. Relativistic effects were included using the Zero-Order Regular Approximation (ZORA).[59] Exchange-correlation effects were described at the BLYP[60,61] and OPBE[62,63] level of theory. Convergence criteria for geometry optimizations were 5×10^{-4} hartree in the total energy, 5×10^{-3} Hartree/Å in the gradients, 5×10^{-3} Å in bond lengths, and 0.25 degrees in bond and dihedral angles.

III. Results and Discussion

A. Fe^{II}−$EDTAH_n$ Complexes. We study here the influence of stepwise ligand protonation on the equilibrium geometry and electronic structure of Fe^{II}/EDTA complexes. Up to eight chelates of general formula $[Fe{\cdot}EDTAH_n]^{-2+n}$ can be generated by considering the five possible protonation states ($n = 0-4$) of the ligand. We neglect situations for the low protonation number ($n = 2$) in which oxygen atoms belonging to carboxylic groups joining at the same nitrogen atom are simultaneously protonated. The eight complexes then are as follows: $[Fe{\cdot}EDTA]^{2-}$, $[Fe{\cdot}EDTAH]^-$ (O′ protonated), $[Fe{\cdot}EDTAH]^-$ (O″ protonated), $[Fe{\cdot}EDTAH_2]$ (O′, O′ protonated), $[Fe{\cdot}EDTAH_2]$ (O″, O″ protonated), $[Fe{\cdot}EDTAH_3]^+$ (O′, O″, O″ protonated), $[Fe{\cdot}EDTAH_3]^+$ (O″, O′, O′ protonated) and $[Fe{\cdot}EDTAH_4]^{2+}$. In all these systems the quintet spin state ($S = 2$, four unpaired electrons) was found to be ∼50 kJ mol^{-1} lower in energy than the triplet ($S = 1$, two unpaired electrons), at the OPBE level of theory, and this in turn to be ∼3 kJ mol^{-1} below the singlet ($S = 0$, no unpaired electrons).

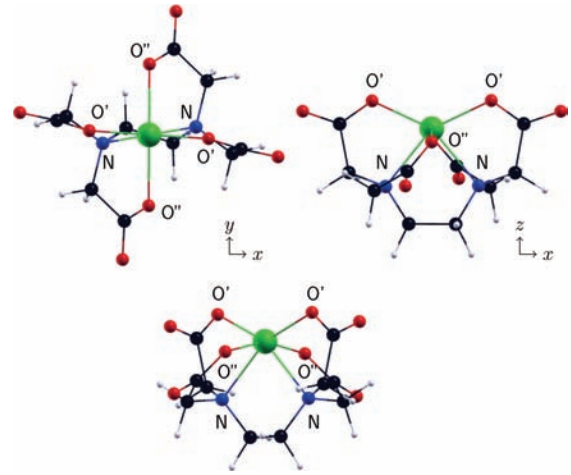

Figure 2. Molecular structures of EDTA-chelated Fe^{II} obtained from geometry optimization, indicating our choice of Cartesian axes. The Fe cation is at the center of each plot, and it is taken as the origin of the coordinate system. Notice each nitrogen atom joins a carboxylic group containing an O′ atom and one containing an O″ atom. The four oxygen atoms coordinated to Fe are regarded as being roughly in a plane, which we indicate as *xy* plane. The *z* axis passes through the midpoint of the N−N axis and the metal ion center. In the upper left panel the midpoint of the N−N axis is behind the Fe, and the *z* axis points toward the reader. The *y* axis is (approximately) defined by the metal ion and the two O″ atoms, and the *x* axis is approximately defined by the metal ion and the O′ atoms. The two upper panels show projections in the *xy* and *xz* planes; the figure on the right is obtained from the one on the left by rotation of 90 ° degrees around the *x* axis, rotating the two N atoms from behind the Fe atom into the plane of drawing. The lower figure is obtained by rotation of the upper right one by ∼45° around the *z* axis so as to better expose the O″ atoms.

For the unprotonated $[Fe{\cdot}EDTA]^{2-}$ complex (see Figure 2, upper left panel) the coordination geometry of the Fe^{II} ion could be described as *distorted octahedral*, with the two nitrogen atoms and two oxygen atoms (indicated as O′) roughly forming the equatorial plane, and the two remaining oxygen atoms (O″) above and below the plane. We will, however, consider here an alternative description of the coordination geometry, in which the four oxygen atoms are considered to be roughly forming the equatorial plane, and the two nitrogens are regarded as a single (pseudo) ligand, see ref 55. Within this convention, the coordination site *trans* to the midpoint of the N−N axis is vacant. If it is occupied with an O ligand, we obtain the EDTA complex of $Fe^{IV}O^{2+}$, which has a very low barrier for hydroxylation reactions owing to the high spin nature of the complex and the weak donor property of the somewhat remote *trans* axial ligand (constituted by the two N atoms), see ref 55. The choice of Cartesian axes corresponding to this way of viewing the complex is indicated in Figure 2. The *x* axis is approximately

(55) Bernasconi, L.; Baerends, E. J. *Eur. J. Inorg. Chem.* **2008**, *2008*, 1672–1681.
(56) *ADF2005.01, SCM*; Theoretical Chemistry, Vrije Universiteit Amsterdam: The Netherlands; http://www.scm.com.
(57) Baerends, E. J.; Ellis, D. E.; Ros, P. *Chem. Phys.* **1973**, *2*, 41–51.
(58) Fonseca Guerra, C.; Snijders, J. G.; te Velde, G.; Baerends, E. J. *Theor. Chem. Acc.* **1998**, *99*, 391–403.
(59) van Lenthe, E.; Baerends, E. J.; Snijders, J. G. *J. Chem. Phys.* **1994**, *101*, 9783–9792.
(60) Becke, A. *Phys. Rev. A* **1988**, *38*, 3098–3100.
(61) Lee, C.; Yang, W.; Parr, R. G. *Phys. Rev. B* **1988**, *37*, 785–789.
(62) Handy, N. C.; Cohen, A. J. *Mol. Phys.* **2001**, *99*, 403–412.
(63) Perdew, J. P.; Burke, K.; Ernzerhof, M. *Phys. Rev. Lett.* **1996**, *77*, 3865–3868.

Table 1. Selected Optimized Bond Distances (Å), Bond and Dihedral Angles (deg) of Fe^{2+}−EDTA Complexes in Different Ligand Protonation States[a]

		$[Fe\cdot EDTA]^{2-}$	$[Fe\cdot EDTAH]^{-}$		$[Fe\cdot EDTAH_2]$		$[Fe\cdot EDTAH_3]^{+}$		$[Fe\cdot EDTAH_4]^{2+}$
			O′	O″*	O′, O*	O″, O″	O′, O′, O″	O″, O″, O′*	
Fe−O	O′	2.075, 2.075	2.070, 5.166	1.998, 1.976	2.645, 2.645	1.962, 1.962	2.271, 2.345	1.902, 2.147	2.102, 2.102
	O″	2.253, 2.253	2.024, 1.964	2.088, 3.613	1.941, 1.941	2.354, 2.354	2.214, 1.918	2.218, 2.280	2.173, 2,172
Fe−N		2.339, 2.339	2.191, 2.625	2.469, 2.340	2.287, 2.287	2.404, 2.404	2.252, 2.334	2.290, 2.469	2.331, 2.330
O′FeO′		129.77	145.30	124.2	137.67	133.05	129.09	131.21	130.96
O″FeO″		162.12	153.18	136.3	176.76	160.94	171.71	160.17	177.36
NFeN		79.05	78.93	76.6	83.65	76.26	82.70	77.82	80.42
Σ CNC		340.59, 340.59	340.43, 337.07	335.93, 338.48	337.90, 337.90	338.77, 338.77	338.25, 340.15	338.17, 339.36	337.69, 337.69
O−O−N−N		13.74, 58.52	8.51, 53.79	17.0, 29.3	13.82, 54.05	15.32, 48.14	16.74, 51.07	17.90, 48.15	20.10, 50.26
C_{br}−N−C−C_{carb}		92.28, 152.85	91.05, 153.06	77.14, 154.75	93.21, 155.10	99.87, 149.90	91.31, 145.49	150.43, 99.58	112.27, 144.46
		92.28, 152.85	96.28, 168.03	84.67, 146.83	93.22, 155.10	99.87, 149.90	109.29, 151.88	143.88, 117.02	112.71, 144.66

[a] O′ and O″ indicate which carboxylic groups are protonated (see text for details; cfr. also Figures 2 and 3). For $[Fe\cdot EDTAH_2]$ we only report parameters for the complexes with carboxylate groups protonated which are *trans* to each other with respect to the metal ion centre. Σ CNC is the sum of the three CNC angles. C_{br}−N−C−C_{carb} is the dihedral angle defined by a carbon atom of the ethylene bridge separating the two nitrogens, a nitrogen, and the two carbons of a carboxylic arm.

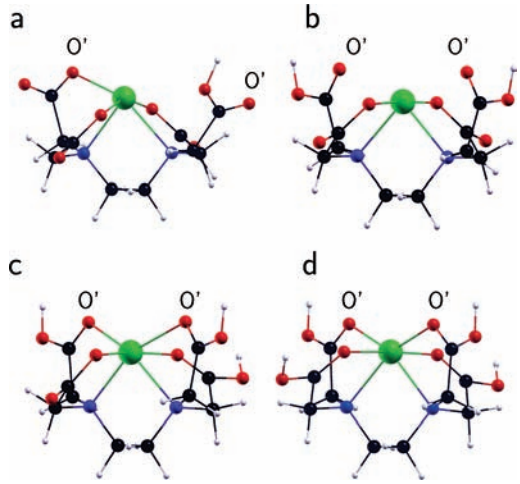

Figure 3. Optimized geometries of $[Fe\cdot EDTAH]^{-}$ (O′ protonated, **a**), $[Fe\cdot EDTAH_2]$ (O′, O′ protonated, **b**), $[Fe\cdot EDTAH_3]^{+}$ (O′, O′, O″ protonated, **c**) and $[Fe\cdot EDTAH_4]^{2+}$ (**d**). The not exhibited structures of $[Fe\cdot EDTAH]^{-}$ (O″ protonated), $[Fe\cdot EDTAH_2]$ (O″, O″ protonated), and $[Fe\cdot EDTAH_3]^{+}$ (O″, O″, O′ protonated) are similar to the corresponding (O′), (O′, O′) and (O′, O′, O″) protonated ones shown here, the protonated carboxylate group(s) always being at larger distance from the metal center than the anionic ones. Orientation is as in the lower panel of Figure 2.

defined by the positions of the metal ion and the O′ atoms, and the *y* axis by the metal ion and the O″ atoms. The *z* axis passes through the midpoint of the N−N axis and the metal ion (and the O of FeO^{2+} if it is present). The geometric data in Table 1 show that in $Fe\cdot EDTA^{2-}$ the O″ FeO″ angle of 162° is not too different from 180°, but the O′FeO′ angle of 130° is relatively acute, as is also visible in Figure 2, bottom panel. The latter angle becomes larger (∼144°) in the FeO^{2+} complex. The FeO′ distance (2.075 Å) is somewhat shorter than the FeO″ distance (2.253 Å). The distance to the N atoms is relatively large (2.34 Å), which accounts for their weak donor ability mentioned above.

1. Equilibrium Structures of the $FeEDTAH_n$ Complexes. The optimized structures of the protonated complexes are shown in Figure 3, and selected geometric parameters are collected in Table 1. In general, protonation decreases the affinity of a carboxylic group for the cation center, largely because of reduced electrostatic interaction. Of the two oxygens of a carboxylic acid group, the nonprotonated oxygen is the one that coordinates to the Fe, but the relative flexibility of the EDTA ligand framework allows the complete protonated carboxylate group (the carboxylic acid group) to move away from the metal ion. This happens to rather different degrees in the various protonated systems.

Singly Protonated Systems. Protonation of $[Fe\cdot EDTA]^{2-}$ to $[Fe\cdot EDTAH]^{-}$ may occur at either an O′ or an O″ arm. We found the two possibilities to yield essentially analogous equilibrium geometries, with one O′ or one O″ open arm respectively, and to be comparable in energy, the O″ protonated configuration being only 9 kJ mol^{-1} lower in energy than the O′ one. In case of protonation at the O′ group, the (nonprotonated) O′ atom loses completely the coordination to the Fe ion, the FeO′ distance increases to 5.166 Å. Protonation of an O″ group also makes the O″ atom move away, but not so far from Fe, 3.613 Å. As may be seen in Table 1, the monoprotonated complex is the only one to exhibit this somewhat peculiar "unbalanced" coordination geometry, with one oxygen at a relatively large distance from the Fe ion and three oxygen atoms at ∼2 Å. The coordination of the metal ion in this system is better described as *pseudo-octahedral*, with three oxygens and one nitrogen (the one at 2.6 Å) in the equatorial plane, the other N (the one at short distance) in axial position and the *trans* axial ligand missing (see panel **a** in Figure 3). To highlight this shift in the coordination of the Fe ion in the monoprotonated complex, which is important in view of the role the monoprotonated system $[Fe\cdot EDTAH]^{-}$ will play in the rest of this paper, we compare in Figure 4**a** and **b** the geometry of the unprotonated and O′ protonated species, respectively. Figure 4 also indicates the axis orientation which we will adopt for the complexes in which the monohydrated species occurs, with either vacant apical site or with H_2O and O_2 as apical ligands: $[Fe\cdot EDTAH]^{-}$, $[Fe\cdot EDTAH\cdot H_2O]^{-}$, $[Fe\cdot EDTAH\cdot O_2\cdot EDTAH\cdot Fe]^{2-}$. With reference to Figure 3, we will label the coordination geometry observed in the monohydrated complexes $[Fe\cdot EDTAH]^{-}$, $[Fe\cdot EDTAH\cdot H_2O]$, and $[Fe\cdot EDTAH\cdot O_2\cdot EDTAH\cdot Fe]^{2-}$ as type **b**, and the coordination geometry in the di-, tri- and fourfold hydrated complexes $[Fe\cdot EDTA]^{2-}$, $[Fe\cdot EDTAH_2]$, $[Fe\cdot EDTAH_3]^{+}$, and $[Fe\cdot EDTAH_4]^{2+}$ as type **a**. As a final comment on the singly protonated system, we note that such an asymmetric Fe^{2+} coordination is not observed in the solid state, where this system crystallizes as $[Fe\cdot(H_2O)_4][Fe\cdot EDTAH\cdot$

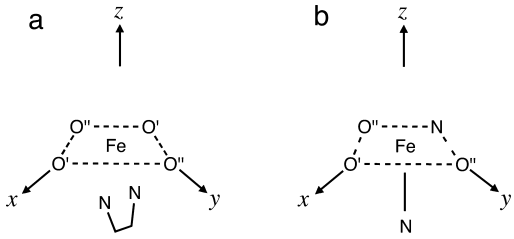

Figure 4. Schematic representation of the Fe^{II} coordination environment and Cartesian axis choice in $[Fe\cdot EDTA]^{2-}$, $[Fe\cdot EDTAH_2]$, $[Fe\cdot EDTAH_3]^{+}$, and $[Fe\cdot EDTAH_4]^{2+}$ (**a**), and in $[Fe\cdot EDTAH]^{-}$ (**b**). Notice in the coordination type **a** the four oxygens (each one belonging to a different carboxylic arm) are considered to be approximately in a plane, and the nitrogen atoms constitute an axial (pseudo) ligand. In the coordination type **b**, one of the O′ atoms has been removed from the coordination sphere, owing to protonation of the corresponding carboxylic arm, and is replaced by one of the nitrogen atoms. The second nitrogen atom acts as a proper axial ligand. In both coordination models, the apical site is vacant.

$(H_2O)]_2$.[64] Besides, we remark that a preference for O″ protonation over O′ is only observed when the apical coordination site *trans* to the nitrogen is vacant; in the presence of a coordinating water molecule (as in the monohydrated $[Fe\cdot EDTAH\cdot H_2O]^{-}$ complex studied in Section IIIA3) or of a dioxygen molecule (as in the dinuclear $[Fe\cdot EDTAH\cdot O_2\cdot EDTAH\cdot Fe]^{2-}$ complex of Section IIIB), O′ protonation appears to be more favorable.

Two-fold Protonation of $[Fe\cdot EDTA]^{2-}$. Two-fold protonation of $[Fe\cdot EDTA]^{2-}$ may occur at the two O′ or two O″ carboxylate groups. Consistent with single-crystal X-ray diffraction studies of the related complex $[Fe\cdot EDTAH_2\cdot H_2O]\cdot 2H_2O$,[64] O′ protonation yields a complex which is more stable, if only by 13 kJ mol^{-1}, than an O″ protonated one. We show in Table 2 a comparison between our calculated equilibrium parameters for $[Fe\cdot EDTAH_2]$ (O′, O′ protonated) and the solid-state data for $[Fe\cdot EDTAH_2\cdot H_2O]\cdot 2H_2O$. Although agreement for most distances and bond angles is evident, larger mismatches are observed for parameters relating to carboxylic arm opening and Fe−O coordination, likely as a consequence of the interaction with the additional water molecules in the crystal (see Figure 3 of ref 64; this coordination geometry is there referred to as *pentagonal-bipyramidal*).

Three-fold Protonation. Three-fold protonation has a rather moderate effect on the symmetry of the metal coordination environment. In particular, all Fe−O distances are within 2.0−2.3 Å, irrespective of the fact that one carboxylic group is unprotonated. This situation clearly contrasts with the highly asymmetric geometry of the monoprotonated ligand complex. The two possible structures (indicated as O′, O′, O″ and O″, O″, O′ in Table 1) again differ in energy by only 5 kJ mol^{-1}, and they have analogous structures.

Full Protonation. Full protonation restores the initial symmetry, with FeO and FeN distances similar to the unprotonated ligand complex. In this situation, notwithstanding the absence of ligand−Fe^{2+} charge−charge interactions, the ligand field stabilization originating from residual electrostatic and orbital interactions is sufficient to prevent $EDTAH_4$ from adopting the free-ligand "open" configuration and consequently losing its chelating ability. According to these results, and consistent with experiment,[47−50] Fe^{2+}/EDTA complexes may therefore be stable in solution even at pH sufficiently low to bring about complete protonation of the ligand. According to our recent theoretical results,[55] such complete protonation of the EDTA complex of FeO^{2+} brings about a very low activation barrier in the gas-phase hydroxylation reaction of methane.

2. Electronic Structure and Orbital Analysis. The energies of the five 3d orbitals of Fe^{2+} (only one of which is doubly occupied in the d^6 high-spin quintet configuration, $S = 2$) are determined by their electrostatic and orbital interaction with two nitrogen atoms and up to four oxygen atoms of protonated or unprotonated carboxylate groups. We also observe that since all systems are in a quintet ground state and all unpaired electrons are localized on the metal ion center, 3d states belonging to the majority spin component (↑ in our calculations) will experience a much larger exchange stabilization. This results in an asymmetric distribution of the spin ↑ and spin ↓ 3d energy levels (see Figures 6 and 7), with the former 2−2.5 eV lower in energy.

Orbital interactions may involve up to 4 *n*-lone pairs and 4 π-lone pairs belonging to the unprotonated O atom of protonated or unprotonated carboxylic groups and the two σ-lone pairs of the nitrogen atoms. The orbitals of the isolated neutral $EDTAH_4$ are displayed in Figure 5, with $EDTAH_4$ in the conformation and orientation of the Fe^{2+} complex as depicted in Figure 3, panel **d**. The highest occupied orbital (HOMO) and almost degenerate second highest occupied orbital (HOMO−1) are plus and minus combinations, respectively, of N σ-lone pair orbitals, the near degeneracy indicating very small overlap of the two N lone pairs. These orbitals lie ∼1.4 eV above the almost degenerate O *n*-lone pairs and ∼2.6 eV above the O π-lone pairs. All these occupied orbitals will have a destabilizing effect on the higher lying 3d orbitals. The most destabilized 3d orbital is always the $3d_{x^2-y^2}$ (only in $FeEDTAH_2$ the d_{xz} is marginally higher). This is because there are always four σ donor lone pairs in the equatorial plane, either four oxygen ones in the type **a** coordination environment, or three oxygens and an N in the type **b** coordination. In the coordination type **a**, there are two N lone pairs straddling the negative *z* axis. These N lone pairs establish σ interactions with suitably oriented 3d orbitals. The $3d_{xz}$ orbital interacts with these N lone pairs via the antisymmetric HOMO−1 and is accordingly destabilized. We find in $FeEDTA^{2-}$ (Figure 6, upper panel) and in the two- to four-fold protonated complexes $FeEDTAH_n^{-2+n}$ (Figure 7), with all type **a** conformations, the d_{xz} indeed high in the 3d spectrum. In all the systems with type **a** coordination, the $3d_{z^2}$ is rather lower than the $3d_{x^2-y^2}$ and $3d_{xz}$. This is because of the limited overlap between the two σ-lone pairs of the two N atoms straddling the negative *z* axis and the lobe of the $3d_{z^2}$ orbital along the $-z$ axis, caused by reduced Fe−N distances (2.3−2.5 Å).

(64) Mizuta, T.; Wang, J.; Miyoshi, K. *Inorg. Chim. Acta* **1995**, *230*, 119–125.

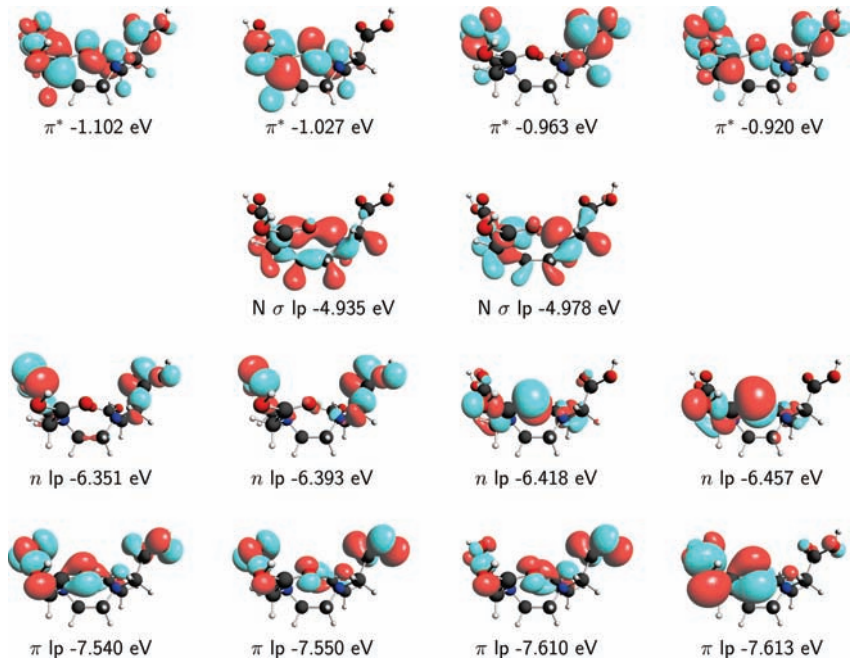

Figure 5. Selected virtual (upper row) and occupied Kohn−Sham orbitals of the free four-fold protonated EDTA ligand, in the conformation of the Fe^{2+} complex of Figure 3**d**. Occupied orbitals involved in the interaction with the metal ion 3d states are the lone pairs of the N atoms (N σ lp), and the *n*- and π-lone pairs of the carboxylate arms (*n* lp and π lp).

Table 2. Comparison between Solid-State X-ray Diffraction Distances (Å) and Bond Angles (deg) for the Complex [Fe·EDTAH$_2$·H$_2$O]·2H$_2$O and Calculated Values for Gas-Phase [Fe·EDTAH$_2$·H$_2$O] O′, O′ Protonated[a]

	experimental [Fe·EDTAH$_2$·H$_2$O]·2H$_2$O	calculated [Fe·EDTAH$_2$] (O′, O′)		experimental [Fe·EDTAH$_2$·H$_2$O]·2H$_2$O	calculated [Fe·EDTAH$_2$] (O′, O′)
Fe1−O3	2.336	2.645 (−0.309)	Fe1−O5	2.082	1.941 (0.141)
Fe1−N8	2.343	2.287 (0.056)	C9−O3	1.213	1.220 (−0.007)
C9−O4	1.309	1.367 (−0.058)	C9−C10	1.503	1.560 (−0.057)
C11−O5	1.270	1.319 (−0.049)	C11−O6	1.238	1.232 (0.006)
C11−C12	1.527	1.561 (−0.034)	N8−C10	1.471	1.478 (0.007)
N8−C12	1.479	1.501 (−0.022)	N8−C13	1.482	1.498 (−0.016)
C13−C13′	1.516	1.546 (−0.030)	O4−H4	0.97	0.984 (−0.014)
O3−Fe1−O3′	147.32	137.67 (9.65)	O3−Fe1−O5	90.62	86.59 (4.30)
O3−Fe1−O5′	95.19	94.48 (0.71)	O3−Fe1−N8	68.59	70.35 (−1.76)
O3−Fe1−N8′	143.99	150.97 (−6.98)	O5−Fe1−O5′	159.28	176.75 (−17.47)
O5−Fe1−N8	77.06	82.74 (−5.68)	O5−Fe1−N8′	86.57	94.82 (−8.25)
Fe1−O3−C9	113.9	106.16 (7.74)	Fe1−O5−C11	120.4	120.10 (0.30)
Fe1−N8−C10	107.2	111.96 (−4.76)	Fe1−N8−C12	105.8	103.26 (2.54)
Fe1−N8−C13	108.8	102.97 (5.83)	O3−C9−O4	123.4	123.77 (−0.37)
O3−C9−C10	121.2	125.69 (−4.49)	O4−C9−C10	115.4	110.52 (4.88)
O5−C11−O6	124.1	126.08 (−1.98)	O5−C11−C12	118.3	115.82 (2.48)
O6−C11−C12	117.6	118.08 (−0.48)	N8−C10−C9	108.2	111.21 (v3.01)
N8−C12−C11	114.9	114.47 (0.43)	N8−C13−C13′	109.9	113.30 (−3.40)
C10−N8−C12	111.0	112.70 (−1.70)	C10−N8−C13	111.7	112.00 (−0.30)
C12−N8−C13	111.9	113.20 (−1.30)	C9−O4−H4	108.2	106.40 (1.80)

[a] Labelling of atoms are as in Figure 3 of ref 64. Differences between experimental and calculated values are given in parenthesis.

An interesting deviation from this general pattern occurs for the monoprotonated $[Fe(EDTAH)(H_2O)]^-$ complex (see Section IIIA3). The coordination type **b** of Figure 4, which prevails in that case, creates a better N lone pair as axial donor located at a rather short distance (∼2.2 Å) from the metal ion along the negative *z* axis. The $3d_{z^2}$ orbital is therefore destabilized, and it appears in the Kohn−Sham spectrum of the monoprotonated complex as the second highest-energy orbital, below the $3d_{x^2-y^2}$ which is destabilized by σ interaction with three oxygens and one equatorial nitrogen. As for the type **a** coordination, the latter is therefore the least stable of the 3d orbitals. However, the $3d_{xz}$ is now less destabilized, since the axial N along the negative *z* axis is a σ donor which does not interact with the $3d_{xz}$. Moreover, the equatorial N is also a σ donor and therefore does not exert a pushing up effect on the $3d_{xz}$, at variance with the π lone pairs of the equatorial oxygens (the equatorial N is, in the type **b** configuration, along the *x* axis, see Figure 4, and therefore affects the $3d_{xz}$). This changed role of the N ligands is an important difference with the type **a** coordination.

As the global HOMO, the highest occupied spin ↓ orbital will be shown to play a crucial role in promoting the formation of dinuclear (peroxo) complexes, acting as donor of one electron to dioxygen. Among all the systems studied here, the O′ monoprotonated $[Fe\cdot EDTAH]^-$ complex is the only one to exhibit a $3d^{\downarrow}_{xz}$ occupation, that is, a $(3d_{xz})^2$ ground

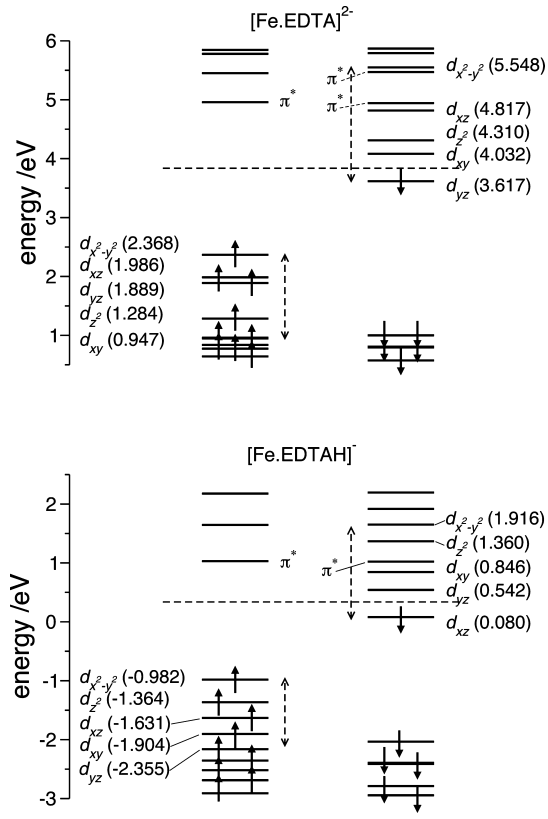

Figure 6. Kohn−Sham energy levels of the unprotonated [Fe•EDTA]$^{4-}$ and O′ monoprotonated [Fe•EDTAH]$^{-}$ complexes. The dashed horizontal line separates virtual from occupied states. Vertical dashed double arrows show the energy range of the 3d manifold in the two spin components. Notice the difference in the energy scale for the two plots. The notation for the d orbitals refers to the axis choice of Figure 4**a** for FeEDTA^{2-} and 4**b** for FeEDTAH^{-}.

state, which will be proved to be the most favorable to give orbital interaction with O_2. Solvation, as described at the COSMO[65−67] level of theory, was found not to affect the orbital ordering or the preference for a given complex for equatorial over axial protonation.

3. Monohydrated [Fe(EDTAH)(H$_2$O)]$^{-}$ Complex. The coordination of a dioxygen molecule to Fe^{2+} as in eq 2 involves the replacement of a water molecule initially coordinated to [Fe•EDTAH]$^{-}$. The ligand substitution can occur for various protonation states of the EDTA ligand ([Fe•EDTA•H$_2$O]$^{2-}$,[Fe•EDTAH•H$_2$O]$^{-}$,and[Fe•EDTAH$_2$•H$_2$O]), but [Fe•EDTAH]$^{-}$ has been shown to bind dioxygen more rapidly than the unprotonated and diprotonated forms. It has been suggested that the higher reactivity of the monoprotonated ligand complex might be related to the increased accessibility of the metal center to the attacking oxygen molecule.[48] This is consistent with our analysis, which has pointed out the peculiarity of the cation coordination in [Fe•EDTAH]$^{-}$ compared to the other complexes: the protonated carboxylate arm moves away over a large distance.

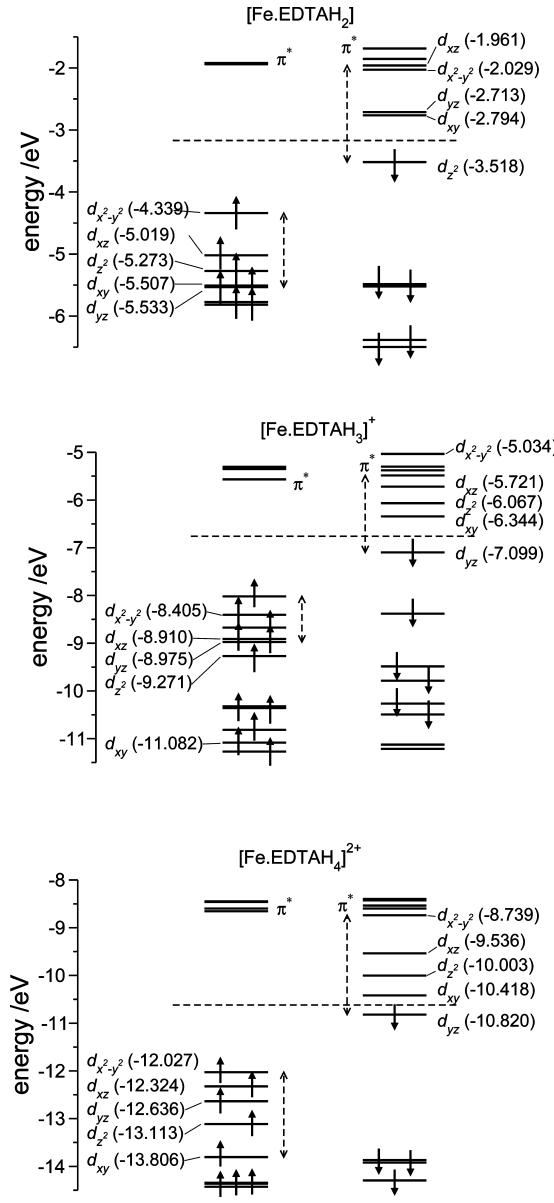

Figure 7. Kohn−Sham energy levels of O′, O′ protonated [Fe•EDTAH$_2$] O″, O″, O′ protonated [Fe•EDTAH $_3$]$^{+}$ and [Fe•EDTAH$_4$]$^{2+}$. The axis orientation is the one of type **a** (see Figure 4**a**).

We studied optimized geometries and electronic structure of the O′ or O″ monoprotonated [Fe•EDTAH•H$_2$O]$^{-}$ monohydrated complexes (O′ and O″ protonated), to asses the importance of an additional water molecule ligand in determining the ground-state spin configuration of [Fe•EDTAH]$^{-}$. We found the energy of the two equilibrium structures to differ by less than 1 kJ mol^{-1}, with a very slight preference for the O′ protonated system (Figure 8). The coordination of the metal ion in this system is similar to [Fe•EDTAH]$^{-}$ and can again be described as distorted octahedral, with three oxygen and one nitrogen atom as equatorial ligands at 2.099, 2.110, and 1.963 and 2.689 Å from Fe^{2+}, respectively, and a nitrogen atom and the water oxygen as axial ligands at 2.231 and 2.462 Å, respectively. The oxygen of the protonated carboxylic arm is again at larger distance from the cation, 3.676 Å. The highest occupied spin ↓ orbital corresponds to the 3d$_{xz}$ which is only

(65) Klamt, A.; Schüürmann, G. *J. Chem. Soc., Perkin Trans.* **1993**, *2*, 799–805.
(66) Pye, C.; Ziegler, T. *Theor. Chem. Acc.* **1999**, *101*, 396–408.
(67) We used the following solvation radii (Å): H 1.30, C 2.00, N 1.83, O 1.72, Fe 2.00.

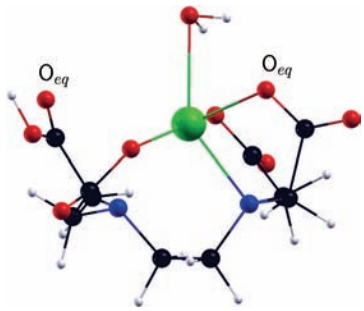

Figure 8. Optimized structure of monohydrated O′ protonated $[Fe\cdot EDTAH]^-$.

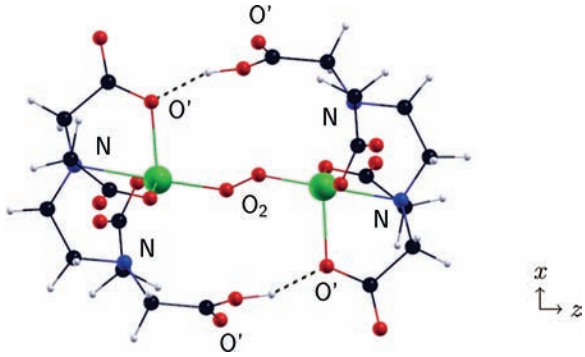

Figure 9. OPBE optimized structure of the oxygenated dinuclear complex $[Fe\cdot EDTAH\cdot O_2\cdot EDTAH\cdot Fe]^{2-}$ O′ protonated, in its $S = 5$ spin state. Dashed lines represent hydrogen bonds between the hydrogen atom of the protonated carboxylic oxygen of one $EDTAH^-$ group and an oxygen atom of an unprotonated carboxylic oxygen belonging to the other $EDTAH^-$ group.

slightly destabilized (0.03 eV) compared to the corresponding orbital in the parent O′ protonated $[Fe\cdot EDTAH]^-$ complex (see discussion in the previous section). This confirms that the $[Fe\cdot EDTAH\cdot H_2O]^-$ complex undergoing ligand substitution in eq 2 is in a $d^{\downarrow}_{xz}$ configuration.

In summary, we have examined in this section the effects of ligand protonation on equilibrium geometries and electronic properties of Fe^{2+}/EDTA complexes. Changes in the Fe coordination environment have been shown to affect not only the relative energies but also the ordering of orbitals belonging to the ligand-field split manifold of metal 3d states, and, in particular, to determine the nature of the HOMO. The singly protonated $[Fe\cdot EDTAH]^-$ complex was found to be peculiar in its geometric and electronic structure. In this system, the coordination geometry of the metal ion is essentially octahedral, with one axial nitrogen ligand and three oxygens and one nitrogen in the equatorial plane, and a vacant apical site. The presence of a nitrogen atom among the equatorial ligands, at higher distance from the metal ion than the three oxygens from carboxylic groups, and of an axial N atom at the $-z$ axis, has been shown to favor a $d^{\downarrow}_{xz}$ ground state. In the next section we will show how this feature may play an essential role in promoting electron transfer from the Fe^{II}/$EDTAH^-$ system in the gas phase.

B. Dinuclear $[Fe\cdot EDTAH\cdot O_2\cdot EDTAH\cdot Fe]^{2-}$ Complex. We consider a dinuclear complex (see Figure 9) obtained from two ($S = 2$) $[Fe\cdot EDTAH]^-$ groups and a dioxygen molecule in its ground state $X^3\Sigma_g^-$, corresponding to the configuration, $(1\sigma_g)^2(1\sigma_u)^2(2\sigma_g)^2(1\pi_u)^4(1\pi_g)^2$. Four unpaired electrons are contributed by each metal center, and two additional unpaired electrons by the oxygen diradical. We optimized the structure of the resulting complex at the OPBE level of theory in various spin states. We found with the OPBE functional the high-spin $S = 5$ state to be lowest in energy, lying some 35 kJ mol^{-1} below $S = 4$. It is interesting to observe that all peroxodiiron(III) species experimentally characterized thus far have an $S = 0$ (i.e., antiferromagnetically coupled) ground state.[13] Whether this finding indicates a genuine peculiarity of the system under study, or whether it should rather be related to limitations of standard DFT will be the subject of future work.[78] Energy differences between spin states may vary with the functional used, and we have used OPBE because this functional has been extensively benchmarked for precisely the energetic ordering of spin states of Fe complexes. Although we will occasionally compare to BLYP, cfr. Table 3, OPBE has been proven to describe accurately structural and electronic properties of several Fe complexes,[68−70] and for this reason we will focus our analysis of the dinuclear complex and of its dissociation on results obtained with the OPBE functional. We also remark that $S = 5$ corresponds to the maximum spin multiplicity compatible with the system (purely ferromagnetic coupling), for which density functional methods are likely to provide a sufficiently accurate description.[71]

The O−O distance in the complex is notably larger (∼0.1 Å) than in the free molecule (1.256 Å calculated; 1.207 Å experimental),[42] consistent with a formal *peroxo* O_2^{2-} group bridging two Fe(III) ions,[72,73] as postulated by van Eldik and co-workers.[47−50] A state with an overall spin quantum number $S = 5$ can describe adequately both a dioxygen *and* a peroxo bridge: the down spin electrons on the Fe ions,

Table 3. Selected Parameters of Optimized Lowest Energy High Spin State Geometries of $[Fe\cdot EDTAH\cdot O_2\cdot EDTAH\cdot Fe]^{2-}$ O′ Protonated in OPBE and BLYP[a]

	OPBE		BLYP		TS
	$S = 4$	$S = 5^*$	$S = 4^*$	$S = 5$	$(S = 4)$
$O-O_{O_2}$	1.443	1.352	1.442	1.398	1.759
$Fe-O_{O_2}$	1.851	1.929	1.894	1.809	1.697
$Fe-O_{EDTA}$	2.054, 2.024	2.042, 2.074	2.133, 2.065	2.129, 2.062	2.131, 2.053
	2.165, 4.452	2.108, 4.377	2.084, 4.318	2.091, 4.334	2.045, 4.441
	2.134, 2.083	2.077, 2.040	2.165, 2.054	2.132, 2.061	2.130, 2.046
	2.065, 4.319	2.113, 1.930	2.023, 4.449	2.087, 4.354	2.044, 2.429
N−Fe	2.471, 2.173	2.446, 2.292	2.332, 2.443	2.338, 2.417	2.455, 2.241
	2.332, 2.441	2.292, 2.440	2.173, 2.469	2.417, 2.339	2.455, 2.236
Fe−Fe	4.542	4.723	4.540	4.700	4.574
Fe−O−O	114.36	122.42	119.65	119.02	121.92
	119.79	122.50	14.27	118.75	121.77
Fe−O−O-Fe	179.72	179.78	179.68	179.56	179.44

[a] An asterisk indicates the ground state. OPBE optimized parameters for the transition state of the O−O cleavage reaction are shown in the rightmost column.

(68) Swart, M.; Groenhof, A. R.; Ehlers, A. W.; Lammertsma, K. *J. Phys. Chem. A* **2004**, *108*, 5479–5483.
(69) Fouqueau, A.; Mer, S.; Casida, M. E.; Daku, L. M. L.; Hauser, A.; Mineva, T.; Neese, F. *J. Chem. Phys.* **2004**, *120*, 9473–9486.
(70) Fouqueau, A.; Casida, M. E.; Daku, L. M. L.; Hauser, A.; Neese, F. *J. Chem. Phys.* **2005**, *122*, 044110.
(71) Noodleman, L. *J. Chem. Phys.* **1981**, *74*, 5737–5743.
(72) The O−O distance observed in the $S = 5$ complex is in fact intermediate between those of a proper "peroxide" adduct (∼1.4−1.5 Å) and of a "superoxide" one (∼1.2−1.3 Å).[73]
(73) Cramer, C. J.; Tolman, W. B.; Theopold, K. H.; Rheingold, A. L. *Proc. Nat. Acad. Sci. U.S.A.* **2003**, *100*, 3635–3640.

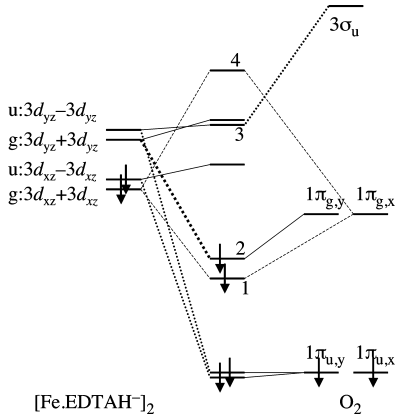

Figure 10. Qualitative orbital interaction diagram for [Fe·EDTAH·O_2·EDTAH·Fe]$^{2-}$ obtained from analysis into the three fragments [Fe·EDTAH]$^-$, [Fe·EDTAH]$^-$, and O_2. Only interactions of selected spin ↓ orbitals of the various fragments are shown. The numbered orbitals are sketched in Figure 11. To the left are the plus and minus combinations of the spin ↓ LUMO ($3d_{xz}$) and LUMO+1 ($3d_{yz}$) levels of the two [Fe·EDTAH]$^-$ complexes, to the right are the spin ↓ HOMO $1\pi_u$ and LUMO $1\pi_g$ orbitals of the oxygen molecule, and the central column are the resulting levels of the complex. The orbital combinations in the complex are labeled 1 ($3d^{\downarrow}_{xz}+1\pi_{g;x}+3d^{\downarrow}_{xz}$), 2 ($3d^{\downarrow}_{yz}+1\pi_{g;y}+3d^{\downarrow}_{yz}$), 3 ($3d^{\downarrow}_{yz}+2\sigma_u-3d^{\downarrow}_{yz}$), 4 ($3d^{\downarrow}_{xz}-1\pi_{g;x}+3d^{\downarrow}_{xz}$). The orbitals 1 and 2 are occupied by electrons originally belonging to the $3d^{\downarrow}_{xz}$ orbitals of the [Fe·EDTAH]$^-$ fragments.

which are paired with up spin electrons in the $3d_{xz}$ orbitals, can be transferred to O_2 where they pair up with the up spin electrons in the π_g shell of O_2, without any change in the overall spin multiplicity, see Figure 4. The arrangement of the two mononuclear [Fe·EDTAH]$^-$ complexes and the dioxygen molecule allows us to adopt the same convention for the orientation of the coordinate system as for the mononuclear complexes, that is, the coordination geometry of the two metal ions is of type **b** (Figure 4). In particular, the O_2 molecule coordinates to the Fe ion of a Fe·EDTAH$^-$ monomer at the vacant coordination site opposite the axial N atom. The O′ and the other N atom, together with the two O″ atoms of one monomer, form the approximate equatorial plane of the monomer, perpendicular to the Fe−Fe axis (O′−Fe−N_{eq} along the *x* axis). The *z* axis runs through the two Fe ions, and the two metal ions and dioxygen lie exactly in a plane (see value of dihedral Fe−O−O-Fe angles in Table 3), corresponding to the *yz*-plane. The oxygen molecule is coordinated to the two metal centers with a geometry which is intermediate between end- (η^1) and side-on (η^2) (Figure 9). The latter fact implies that the interaction of dioxygen with the metal centers via a δ-bond, which is possible in η^2 coordination,[73] is effectively precluded. As we will discuss below, the empty spin ↓ $1\pi_{g;x}$ and $1\pi_{g;y}$ (antibonding π^*) orbitals and, to a lower extent, the empty lying $3\sigma_u$ orbital will in our case be involved in the O_2−Fe bonding. The occupation of Fe−O bonding orbitals, along with the presence of two hydrogen bonds between the protonated arm of one EDTAH ligand and an unprotonated one of the facing ligand, counterbalances the electrostatic repulsion between the two negatively charged [Fe·EDTAH]$^-$ complexes, and stabilizes the dinuclear system.

The orbital interactions leading to the Fe−O_2 bonding are depicted in Figures 10 and 11. We indicate as $1\pi_{g;x}$ and $1\pi_{g;y}$ the antibonding O_2 π^* orbitals whose lobes are in the *xz*-plane and perpendicular to it (in the *yz* plane), respectively. In triplet O_2 the up spin π_g orbitals are occupied, the down spin counterparts are unoccupied and act as acceptor orbitals. The next higher orbital on O_2 is the empty $3\sigma_u$, whose energy is, however, too large for it to act efficiently as an acceptor. The Fe−O_{O_2} orbital interaction originates from the following main contributions. The plus combination (*gerade*) of the two $3d_{xz}$ orbitals interacts with $1\pi_{g;x}$. Since the $1\pi^{\downarrow}_{g;x}$ is relatively low lying with respect to the $3d^{\downarrow}_{xz}$, the resulting orbital has large $1\pi^{\downarrow}_{g;x}$ character (53%, see Figure 10). The resulting orbital, which is the main one responsible for the Fe → O_2 electron transfer, is shown in Figure 6, top panel. Second, the $1\pi_{g;y}$ can interact with the plus combination of $3d_{yz}$ orbitals, which are not much higher in energy than the $3d_{xz}$, see Figure 5. This also leads to a stabilization of the $1\pi_{g;y}$ orbital, which is however not as large as for the $1\pi_{g;x}$ because the fragment $3d_{yz}$ + $3d_{yz}$ orbital is at higher energy. The stabilized $1\pi_{g;y}$ receives the electron of the $3d_{xz}$ − $3d_{xz}$ orbital, thus also the second electron in the $3d_{xz}$ orbitals moves to a predominantly O_2 orbital. Finally, the empty O_2 $3\sigma^{\downarrow}_u$ orbital can stabilize lower lying *ungerade* orbitals of the dinuclear iron fragment, but it mixes slightly with the highest *ungerade* 3d orbitals, see, for example, orbital 3 as pictured in Figure 10. These highest *ungerade* 3d orbitals are empty, so the mixing has no effect. Orbital 3 is displayed in Figure 12, bottom panel, which clearly shows the small admixture of $3\sigma_u$ character and the dominating $3d_{yz}$ character. The overall orbital interaction thus formally results in the donation of one electron from each metal ion to dioxygen, creating a peroxo ion O_2^{2-}, with the two Fe^{III} now carrying five unpaired electrons each, as depicted in the lower panel of Figure 13.

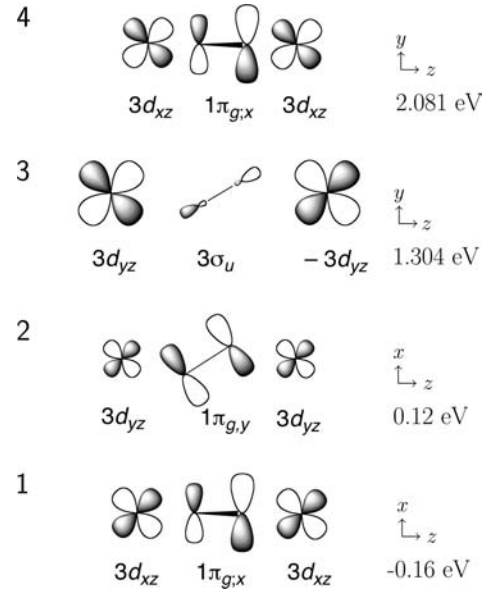

Figure 11. Schematic representation of the orbital combinations 1−4 of Figure 10 and orbital energies. Notice orbitals 1 and 4 are projected in the *xz* plane, orbitals 2 and 3 in the *yz* plane.

C. Formation of $Fe^{IV}O^{2+}$ Species from [Fe·EDTAH·O_2·EDTAH·Fe]$^{2-}$ Dissociation. We now turn to the dissociation of the O−O bond, to determine if this is a viable route to $Fe^{IV}O^{2+}$ species. The dissociation of the O−O bridge

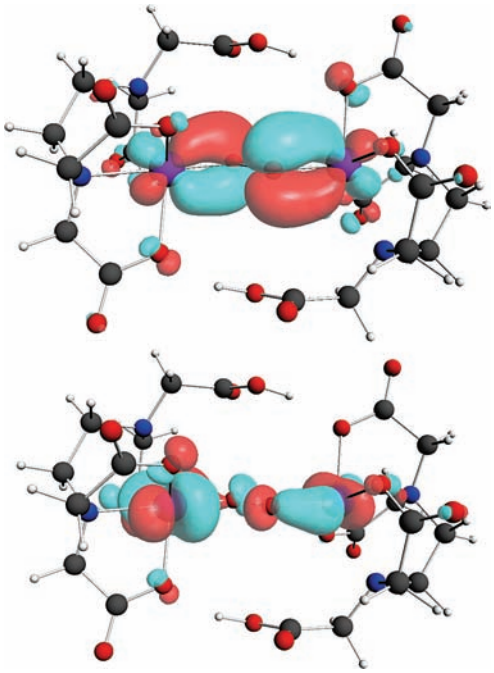

Figure 12. OPBE Kohn−Sham eigenvectors corresponding to the molecular orbitals 1 (above) and 3 of $[Fe{\cdot}EDTAH{\cdot}O_2{\cdot}EDTAH{\cdot}Fe]^{2-}$. See also Figures 10 and 11. Orientation similar to Figure 9.

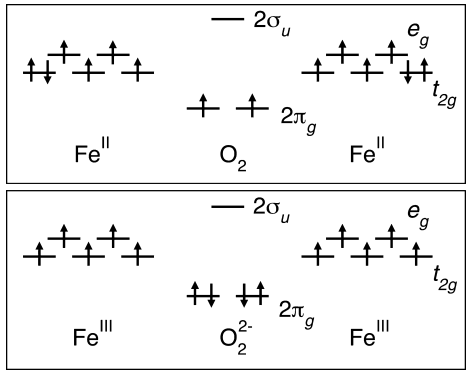

Figure 13. Simplified representation of two possible spin configurations with overall spin quantum number $S = 5$ for two Fe ions in a weak octahedral ligand field with a bridging O_2 diradical.

in $[Fe{\cdot}EDTAH{\cdot}O_2{\cdot}EDTAH{\cdot}Fe]^{2-}$ was induced by performing a series of structural optimizations at fixed values of the O−O distance. A similar approach has been used in recent theoretical studies of oxygen activation in the active sites of methane monooxygenase, ribonucleotide reductase[74−76] and tyrosinase.[77] We show the evolution of the total energy of the complex as a function of the O−O distances for the two lowest energy spin states, computed at the OPBE level of theory in Figure 14. The complex, initially in the $S = 5$ state, undergoes a transition to the $S = 4$ state, with the crossing between the two spin surfaces occurring at ∼1.6 Å. The system evolves from a (formally) superoxo/peroxo dinuclear system to a pair of high-spin ($S = 2$) *oxo* complexes, $[FeO{\cdot}EDTAH]^-$, as the O−O distance is forced

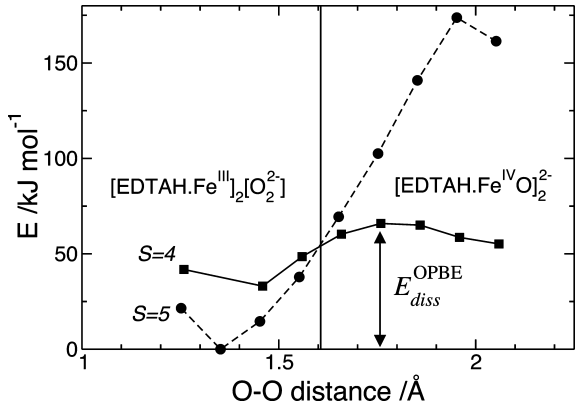

Figure 14. Total energy of the $S = 5$ and $S = 4$ spin states of $[Fe{\cdot}EDTAH{\cdot}O_2{\cdot}EDTAH{\cdot}Fe]^{2-}$ as a function of the O−O distance during bond cleavage, computed at OPBE level of theory. E_{diss}^{OPBE} is the dissociation barrier of the O−O bond, defined by the difference between the optimized $S = 5$ structure and the maximum of the $S = 4$ dissociation curve. Crossing between the $S = 5$ and $S = 4$ energy surfaces, formally describing a *peroxo* dinuclear and a pair of *oxo* $[FeO{\cdot}EDTAH]^-$ complexes respectively, occurs at ∼1.60 Å and is indicated by a vertical line.

to increase. The activation barrier ΔE_{diss}^{OPBE} (disregarding entropic effects) is therefore given by the difference between the $S = 4$ energy curve at its highest point and the energy of the optimized $S = 5$ complex; it amounts to 65.8 kJ mol^{-1}. This value is rather close to the energy of O_2 cleavage in the conversion of compound **P** into compound **Q** of methane monooxygenase computed by Siegbahn on the basis of hybrid DFT calculations (71.5 kJ mol^{-1}),[75] which was found to be in good agreement with the available experimental evidence. The O−O cleavage was in the latter case shown to occur on the ferromagnetic $S = 5$ ground-state spin surface of the bent peroxo complex **P** by symmetric stretching of the O−O bond, until a planar bis(μ-oxo) structure was reached. This was found to be followed by a transition to an antiferromagnetic $S = 0$ state to yield the final compound **Q** model (see Figure 5 of ref 75). A similar O_2 activation mechanism has been proposed for a model of the dicopper complex of tyrosinase.[77]

At variance with these cases, the dissociation of $[Fe{\cdot}EDTAH{\cdot}O_2{\cdot}EDTAH{\cdot}Fe]^{2-}$ in either the $S = 5$ or $S = 4$ state does not bring about notable deviations from Fe−O−O−Fe planarity, fluctuations about the average dihedral angle during the dissociation (∼179°) being rarely as large as ∼1°. During the first stages of the dissociation the Fe−Fe distance is ∼0.2 Å larger in the purely ferromagnetic state, and the transition to the $S = 4$ surface occurs when the Fe−Fe distances are the same in the two spin states (Figure 15). On the $S = 4$ surface the Fe−O distances decrease monotonically as the O−O bond is stretched, consistent with the formation of two equivalent $Fe^{IV}O$ bonds of length ∼1.6 Å. In the $S = 5$ state, a dissociation in two equivalent moieties does not seem to be achievable, as the O−O group rearranges so that both O atoms are closer to one Fe ion than to the other. This situation corresponds to a stretched O_2 molecule in η^2 coordination to one of the Fe ions.[78] The O_2 dissociation on the $S = 5$ surface occurs with an overall barrier of ∼175 kJ mol^{-1}.

Concentrating now on the $S = 4$ surface, we show the structure of the O−O cleavage transition state ($S = 4$) in

(74) Siegbahn, P. E. M.; Crabtree, R. H.; Nordlund, P. *J. Biol. Inorg. Chem.* **1998**, *3*, 314–317.
(75) Siegbahn, P. E. M. *Inorg. Chem.* **1999**, *38*, 2880–2889.
(76) Siegbahn, P. E. M. *J. Biol. Inorg. Chem.* **2001**, *6*, 27–45.
(77) Lind, T.; Siegbahn, P. E. M.; Crabtree, R. H. *J. Phys. Chem. B* **1999**, *103*, 1193–1202.

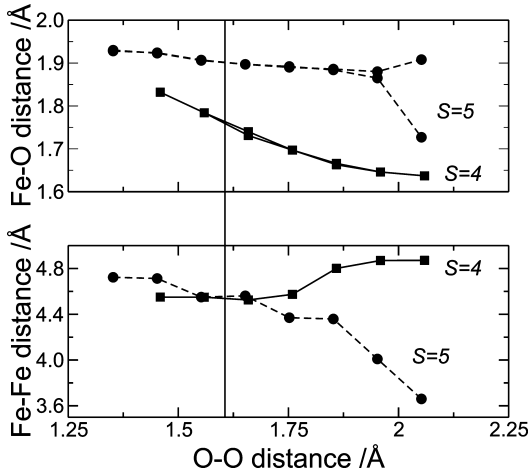

Figure 15. Evolution of Fe−O and Fe−Fe distances in the $S = 5$ and $S = 4$ spin states as a function of the O−O distance during constrained dissociation of $[Fe{\cdot}EDTAH{\cdot}O_2{\cdot}EDTAH{\cdot}Fe]^{2-}$. The lowest O−O value shown corresponds to the optimized distance in each spin state. The vertical line crossing the two panels represents the O−O distance at which the $S = 5$ and $S = 4$ energy surfaces cross, see also Figure 14. The top panel presents the distances of Fe_1 and Fe_2 to the nearest O. For most O−O distances these Fe−O distances are equal, but at the longest O−O distance the O_2 rotates to become perpendicular to the Fe−Fe axis, and is η^2 coordinated with fairly short Fe_1−O distances to Fe_1, and larger Fe_2−O distances to Fe_2. The Fe−Fe distance at that point shortens, see lower panel.

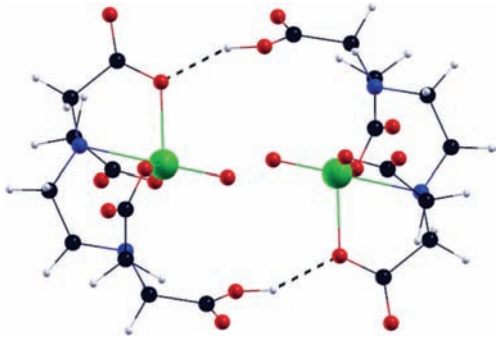

Figure 16. Optimized structure of the transition state of the O−O cleavage reaction in $[Fe{\cdot}EDTAH{\cdot}O_2{\cdot}EDTAH{\cdot}Fe]^{2-}$. Orientation as in Figure 9. See also Table 3.

Figure 16 (see also Table 3). Quite remarkably the overall structure of the complex and the coordination geometry of the metal centers are little affected by the stretching of the O−O bond. This structural rigidity may largely originate from the presence of the two hydrogen bonds between the $[FeO{\cdot}EDTAH]^-$ components, which may hinder rotation along the Fe−Fe bond and constrain the O_2 molecule to lie in a plane with the two metal ions. Again this fact indicates the importance of the protonation state of the EDTA ligand in favoring the formation (and later on dissociation) of a dinuclear complex. The Mulliken spin densities on the Fe ions are 3.5, which is consistent with the value expected for two Fe^{IV} ions.[75] The spin densities on the O atoms initially belonging to the dioxygen molecule are reduced to 0.2, indicative of two closed shell oxide ions with sizable covalent interactions with the metal ions. This confirms that the transition state of the O−O cleavage reaction in $[Fe{\cdot}EDTAH{\cdot}O_2{\cdot}EDTAH{\cdot}Fe]^{2-}$ may be formulated as a pair of incipient $[FeO{\cdot}EDTAH]^-$ complexes bound by hydrogen bonds. The final step in the dissociation of the $[Fe{\cdot}EDTAH{\cdot}O_2{\cdot}EDTAH{\cdot}Fe]^{2-}$ complex to yield two isolated $[FeO{\cdot}EDTAH]^-$ thus requires overcoming a barrier at most as large as the energy of two hydrogen bonds (~40 kJ mol^{-1}), although possibly much reduced by repulsive electrostatic interactions between the two moieties. In solution this process may be assisted by one or more water molecules belonging to the first solvation shell of the complex, which may form hydrogen bonds with the oxygen atoms of the unprotonated carboxylic arms or with the hydrogens of the protonated ones, thus effectively "opening" the complex and promoting the separation of the $[FeO{\cdot}EDTAH]^-$ moieties. Work is currently in progress based on ab initio molecular dynamics simulations to verify the importance of surrounding water molecules on the kinetics of $[Fe{\cdot}EDTAH{\cdot}O_2{\cdot}EDTAH{\cdot}Fe]^{2-}$ dissociation.

It has been pointed out[75,79] that DFT methods often yield gravely unbalanced descriptions of the relative energies of different spin states. This is already the case for hybrid DFT which tends to favor slightly states with higher spin multiplicity, and the problem becomes critical whenever pure density functionals are used. In chemical processes involving one spin energy surface, this problem only affects predictions about the thermodynamics of the reaction; kinetic properties may still be computed satisfactorily. If however, as in our case, a spin transition occurs at some intermediate stage of the reaction, the calculation of kinetic barriers may also suffer from large inaccuracies. For this reason, despite increasing evidence in the literature supporting the good quality of OPBE results regarding relative spin state stabilities of transition metal complexes,[54,68−70] we believe that our estimate of the O−O dissociation barrier in $[Fe{\cdot}EDTAH{\cdot}O_2{\cdot}EDTAH{\cdot}Fe]^{2-}$ should be taken with considerable caution. A more reliable estimate of relative spin-state energies during O−O dissociation, based on proper incorporation of exchange coupling,[71] will be the subject of a future publication.[78] Interestingly, we found, however, that the constrained dissociation of O_2 in a hypothetical model complex of composition $[(H_2O)_5{\cdot}FeO_2{\cdot}Fe(H_2O)_5]^{4+}$ occurs as in $[Fe{\cdot}EDTAH{\cdot}O_2{\cdot}EDTAH{\cdot}Fe]^{2-}$ (Figure 17). Initially, the complex is in a ferromagnetically coupled ground state, with the $S = 4$ state some 40 kJ mol^{-1} higher in energy, similar to $[Fe{\cdot}EDTAH{\cdot}O_2{\cdot}EDTAH{\cdot}Fe]^{2-}$. As the O−O bond is being cleaved, this system evolves to two high spin ($S = 2$) $[(H_2O)_5FeO]^{2+}$ complexes (total $S = 4$). A crossing to the $S = 4$ energy surface occurs again at an O−O distance of ~1.6 Å. In this case the overall barrier is, however, of the order of 120 kJ mol^{-1}, that is, roughly twice as large as in $[Fe{\cdot}EDTAH{\cdot}O_2{\cdot}EDTAH{\cdot}Fe]^{2-}$, and this is mainly a consequence of the much more pronounced dependence of the energy of the $S = 4$ state on the O−O distance (cfr. Figure 14). Although rather indirectly, comparison of $[Fe{\cdot}EDTAH{\cdot}O_2{\cdot}EDTAH{\cdot}Fe]^{2-}$ and $[(H_2O)_5{\cdot}FeO_2{\cdot}Fe(H_2O)_5]^{4+}$ thus lends support to the hypothesis that EDTA-coordinated Fe^{2+} may act as a better electron donor to O_2 than a solvated Fe^{2+} ion, and thus render the reduction of a

(78) Belanzoni, P.; Bernasconi, L.; Baerends, E. J., in preparation.
(79) Siegbahn, P. E. M.; Blomberg, M. R. A. *Annu. Rev. Chem.* **1999**, *50*, 221–249.

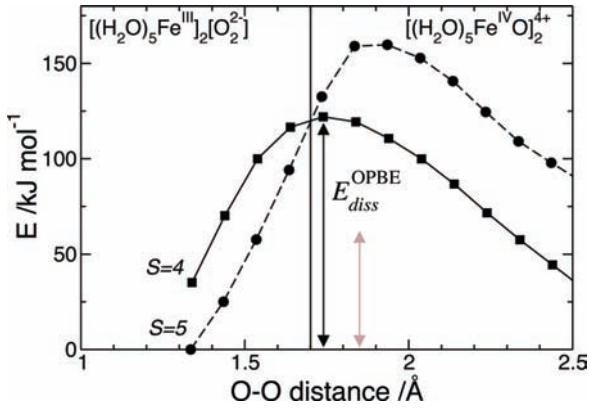

Figure 17. Total OPBE energy of the $S = 5$ and $S = 4$ spin states of $[(H_2O)_5 \cdot FeO_2 \cdot Fe(H_2O)_5]^{4+}$ as a function of the O−O distance during bond cleavage. The vertical line indicates the crossing of the two spin energy surfaces. The dissociation barrier of the O−O bond E_{diss}^{OPBE} (vertical black arrow) is compared to the corresponding quantity for $[Fe \cdot EDTAH \cdot O_2 \cdot EDTAH \cdot Fe]^{2-}$ (gray arrow).

coordinated oxygen molecule kinetically more favorable. We also note that starting from BLYP optimized $[Fe \cdot EDTAH \cdot O_2 \cdot EDTAH \cdot Fe]^{2-}$, the O−O bond dissociation can be made to occur entirely on the $S = 4$ energy surface, with an overall barrier of ∼15 kJ mol^{-1}. With this functional, the $S = 5$ surface is always at least ∼10 kJ mol^{-1} higher in energy than the $S = 4$ one.

In summary we have shown in this section that the formation of a dinuclear Fe/EDTA/O_2 complex is favored by a ligand environment promoting double occupation of a metal $3d_{xz}$ orbital whose symmetry and orientation allow it to establish π interaction with the $1\pi_{g;x}$ molecular orbital of O_2. The two down spin electrons in the $3d_{xz}$ orbitals of the iron fragments occupy plus and minus combinations of the $3d_{xz}$ orbitals in the dinuclear complex. One of these two electrons occupies the stabilized (by interaction with $3d_{xz}+3d_{xz}$) down spin $1\pi_{g;x}$ orbital of O_2, which was originally empty. The second down spin $1\pi_g$ orbital, $1\pi_{g;y}^{\downarrow}$, is stabilized by interaction with $3d_{yz}+3d_{yz}$, and receives the down spin electron from the $3d_{xz}-3d_{xz}$. Through these interactions one electron per metal ion is formally donated to (or involved in a covalent bond with) dioxygen. In its $S = 5$ ground state, consistent with the natural active site models of refs,48, 49 the dinuclear $[Fe \cdot EDTAH \cdot O_2 \cdot EDTAH \cdot Fe]^{2-}$ system can be formulated as two Fe^{III} ions bridged by a peroxo group. During O−O bond cleavage a transition to the $S = 4$ spin state is observed, and the system evolves toward two high spin ($S = 2$) $[FeO \cdot EDTAH]^-$ complexes. The dissociation of the complex following O−O cleavage involves the breaking of two hydrogen bonds, and, in solution, the latter process is likely to be assisted by one or more surrounding solvent molecules. It might be speculated that in the case of a dinuclear system obtained from two $[Fe \cdot EDTAH_2]$ complexes (which also possesses a doubly occupied 3d orbital of suitable orientation for interaction with dioxygen) O−O cleavage might similarly occur, but the cost of cleaving four hydrogen bonds and the absence of electrostatic repulsion between the two $[FeO \cdot EDTAH_2]$ components would make the dissociation of the complex energetically unfavorable. Formation of dinuclear complexes may conversely be hindered or even prevented from occurring for higher EDTA protonation states, because of the lack of suitable donor/acceptor patterns for hydrogen bonds between the two complex moieties.

D. Summary and Conclusions. We have analyzed the effects of ligand protonation on structure and electronic properties of Fe^{II}/EDTA compounds in the gas phase. We have shown that protonation of one or more carboxylic arms results in reduced affinity for the metal center, which in turn brings about important changes in the relative energies and ordering of the ligand field split manifold of 3d states on the metal ion. In only one case, namely $Fe \cdot EDTAH^-$, ligand relaxation leads to a large displacement of one carboxylic acid arm away from the metal ion. The ligand environment rearranges to again a pseudo-octahedral coordination of the metal ion, with three oxygens and one nitrogen as equatorial ligands (type **b** coordination, see Figure 4). This ligand environment leads to low-lying $3d_{xz}$ and $3d_{yz}$ orbitals in the down-spin manifold. In the monoprotonated system, $[Fe^{II}EDTAH^{3-}]^-$, the $3d_{xz}$ is lowest and is occupyed by the one available down-spin electron. We have shown that the electronic structure of the monoprotonated system is particularly suitable to give orbital interactions with an oxygen molecule so that the dinuclear $[Fe \cdot EDTAH \cdot O_2 \cdot EDTAH \cdot Fe]^{2-}$ system can be formed.

We have examined the electronic structure of the dinuclear $[Fe \cdot EDTAH \cdot O_2 \cdot EDTAH \cdot Fe]^{2-}$ whose occurrence has been invoked (but so far not conclusively proved) in mechanistic studies of Fe^{II}/Fe^{III} autoxidation in solution, and we have confirmed the postulated formation of a peroxo ion bridging two Fe^{III} centers. Remarkably, at variance with all known peroxodiiron(III) systems characterized so far, we found the resulting peroxodiiron(III) complex to exhibit an $S = 5$ ground state, indicating ferromagnetic coupling between the spin moments of the two Fe(III). We have studied the homolytic breaking of the peroxo bridge in this complex, which has been shown to involve a crossing from an initial ferromagnetic ground state to a lower multiplicity $S = 4$ state. Once the bond is cleaved, the latter state describes two *high spin* ($S = 2$) $[FeO \cdot EDTAH]^-$ units held together by two hydrogen bonds. The generation of chelated ferryl species from dioxygen proceeds through a mechanism similar to the one proposed, for example, for methane monooxygenase, and, at least at the OPBE level of theory, with comparable cleavage barriers. However it differs from the latter in the fact that the transition to a lower spin state occurs well before the transition state is reached. Also, the final state is not the antiferromagnetically coupled $S = 0$ state, as in methane monooxygenase but rather a state of intermediate multiplicity ($S = 4$), corresponding to two ferromagnetically coupled $S = 2$ Fe^{IV} (d^4) centers.

Our results, both at the OPBE and BLYP level of theory, suggest that potentially catalytically active chelated $Fe^{IV}O$ species may be generated in Fe/EDTA/O_2 systems. The C−H activation properties of the (protonated) EDTA complexes $[Fe^{IV}(EDTAH_n)O]^{-2+n}$ in alkane hydroxylation reactions has already been studied in ref 55. Work is also in progress to study various issues relating to the electronic structure of

$[Fe \cdot EDTAH \cdot O_2 \cdot EDTAH \cdot Fe]^{2-}$, in particular the ferromagnetic and antiferromagnetic interactions between the metal centers in the $S = 4$ and $S = 5$ states, and to study the electronic structure origin of the remarkable difference in the O_2 cleavage processes for the $S = 4$ and $S = 5$ reaction pathways.[78]

Acknowledgment. This work was supported by the Dutch National Research School Combination "Catalysis by Design" (NRSC-C). Computer resources were provided by The Netherlands' Scientific Research Council (NWO) through a grant from Stichting Nationale Computerfaciliteiten (NCF).

IC800998N